Full Color Tunable Photonic Crystal from Crystalline Colloidal Arrays with an Engineered Photonic Stop-Band

Moon Gyu Han, Chang Gyun Shin, Seog-Jin Jeon, HongShik Shim, Chul-Joon Heo, Haishun Jin, Jung Woo Kim,* and SangYoon Lee*

The advancement of display technology has played an important role in improving the quality of our daily lives. Due to recent growing interest in mobile and e-book devices, there are new demands for a display with excellent outdoor readability, low power consumption, and reduced eye-fatigue, which has lead to research on reflective displays.[1–3] However, significant work remains to develop a reflective display that can provide a bright and full-color image comparable to printed media with almost zero-power consumption. One promising way to realize this goal is to express full color in a single pixel, which can potentially provide a threefold increase in color brightness over a conventional display composed of red–green–blue (RGB) pixels.[4] To this end, a tunable photonic crystal has recently been demonstrated as a new class of display element, which allows the full-color emission from a single pixel under a broad range of ambient lighting conditions.[5–8] In addition, the so-called structural colors from photonic crystals have advantageous features such as brilliancy and color vividness[9,10] as is commonly observed in nature, e.g., in Morpho-butterflies and beetles.[11,12]

The structural color of a photonic crystal is the result of the interference of light with its periodic structure; the color can be tuned by modulating the periodicity and/or refractive index of the photonic crystal.[13] Modulation of the lattice constant is more favorable for full-color expression than modulation of the refractive index given the potential for large lattice constant modulations relative to experimentally available refractive index modulations. Photonic crystals formed using crystalline colloidal arrays are particularly attractive for investigations on lattice constant manipulation given that the lattice constant and particle ordering is primarily controlled by relatively soft electrostatic interactions between the particles.[14–16] The particles are separated by the solvent phase, and thus large changes in particle–particle separation is possible. However, crystalline colloidal arrays usually exhibit a narrow bandwidth owing to the low refractive index contrast between the particles and the matrix/dispersion medium. Since the total amount of light reflected by a reflective display under ambient light conditions is proportional not only to peak value but also to the bandwidth of the reflectance spectrum, practical reflective display devices require both broader bandwidth and higher peak value for enhanced brightness. As the width of the spectrum can be modulated through engineering the refractive index contrast,[17] one strategy for increasing the total amount of reflected light from the device is to design a system with both high-refractive index contrast and enhanced long-range order. For applications, the system must also exhibit full-color tunability.

Although the fabrication of photonic crystals with high-refractive index materials has long been the subject of research aimed at realizing a wider photonic bandgap,[18] only a limited number of materials including TiO_2, ZnS, ZnO, and ZrO_2 possess both a high refractive index and transparency in the visible wavelength suitable for optically active photonic crystals. Perhaps due to the limited subset of materials available, there has been little success in creating high quality crystalline colloidal arrays which exhibit long-range order from high refractive index materials.[19] This may not only be due to difficulty in preparing highly monodispersed particles from these materials owing to a general tendency for polydispersed particles to form as a result of continuous nucleation during the synthetic process, but also due to the high density of the particles (e.g., 4.23 g cm^{-3} for TiO_2 and 4.09 g cm^{-3} for ZnS, compared with 1.0 and 2.0 g cm^{-3} for polystyrene and silica, respectively), which hampers the formation of crystalline arrays and makes the colloidal particles tend to sediment from the suspension. Finally, the lack of a strong surface charge on the particles, a basic requirement for self-assembly of the particles through electrostatic repulsions, hinders the formation of crystalline colloidal arrays.

To produce crystalline colloidal arrays from high refractive index particles, therefore, the significant challenge of preparing highly charged, monodispersed particles has to be overcome. Due to this difficulty, to date, there has been no report on the dynamic manipulation of a stop-band of a photonic crystal formed through the long-range self-assembly of high refractive index particles by proper stimuli such as an electric field. Here, we report successful tuning of the stop-band width through manipulating the refractive index of a colloidal particle. This achievement represents a significant step toward engineering materials for specific applications. In addition, we have achieved electrical modulation of the photonic stop-band of a colloidal crystal composed of silica-coated ZnS particles dispersed in deionized water for the first time, making it possible to utilize this system for an active tunable photonic color display devices. A schematic representation of the procedure for the fabrication of the highly charged and high refractive index core–shell

Dr. M. G. Han, Dr. C. G. Shin, Dr. S.-J. Jeon, H. Shim, Dr. C.-J. Heo, H. Jin, Dr. J. W. Kim, Dr. S. Y. Lee
Display Device Lab.
Samsung Advanced Institute of Technology
Samsung Electronics
Giheung-gu, Yongin-si, Gyeonggi-do 446-712, South Korea
E-mail: moongyu.han@samsung.com;
jwkim67@samsung.com

DOI: 10.1002/adma.201203211

© 2012 WILEY-VCH Verlag GmbH & Co. KGaA, Weinheim

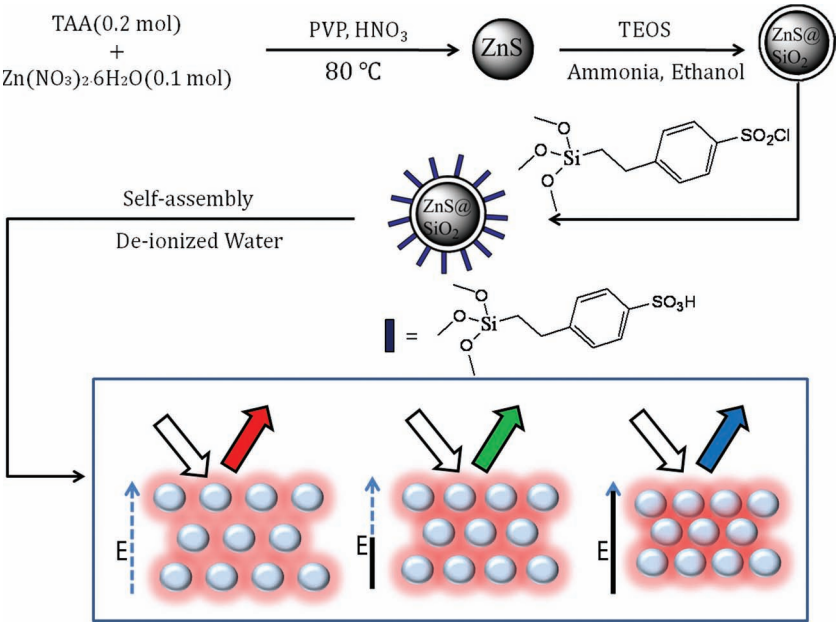

Scheme 1. Schematic illustration showing the procedure for forming negatively charged ZnS–silica core–shell particles: PVP-stabilized ZnS is coated with silica, followed by chemical functionalization. The resulting particles are organized into a periodic structure in deionized water to form a crystalline colloidal array. The photonic structural color is systematically tuned from red to blue by manipulating the interparticle distance with increasing electrical potentials.

nanoparticle and the overall procedures for tuning the photonic stop-band are given in **Scheme 1**.

ZnS is an important inorganic material with light-emitting[20] and magneto-optical properties.[21] Therefore, there have been many reports of the production of ZnS nanoparticles with diameters less than 10 nm. However, due to the difficulty noted earlier in controlling the growth of ZnS crystals, only a few[22–24] have reported the synthesis of ZnS particles with sub-micrometer diameters suitable for creating photonic crystals operating in the visible regime. We successfully synthesized ZnS particles through the homogeneous nucleation of ZnS from zinc nitrate and thioacetamide (TAA) precursors using poly(vinylpyrrolidione) (PVP) both as a structure-directing agent and a stabilizer for the growing ZnS. Monodispersed spherical ZnS particles from 50 to 500 nm were produced with minimal surface roughness with the help of the polymeric stabilizer, PVP. The particle size and the morphology were easily controlled, and particles with the desired diameters were obtained by manipulating the amount of PVP, nitric acid, and the temperatures used in the synthetic recipe. Among the various sized particles, we focused on those with diameters around 100 nm to obtain crystalline colloidal arrays that exhibit a photonic stop-band in the visible region. We discovered that PVP not only effectively aids the growth of uniform sized particles, but also prevents the agglomeration of the growing particles.[25]

Figure 1a,b illustrate the morphologies of representative ZnS particles with an average diameter of 100 nm (synthesized at 80 °C). The ZnS particles appear monodisperse, which was

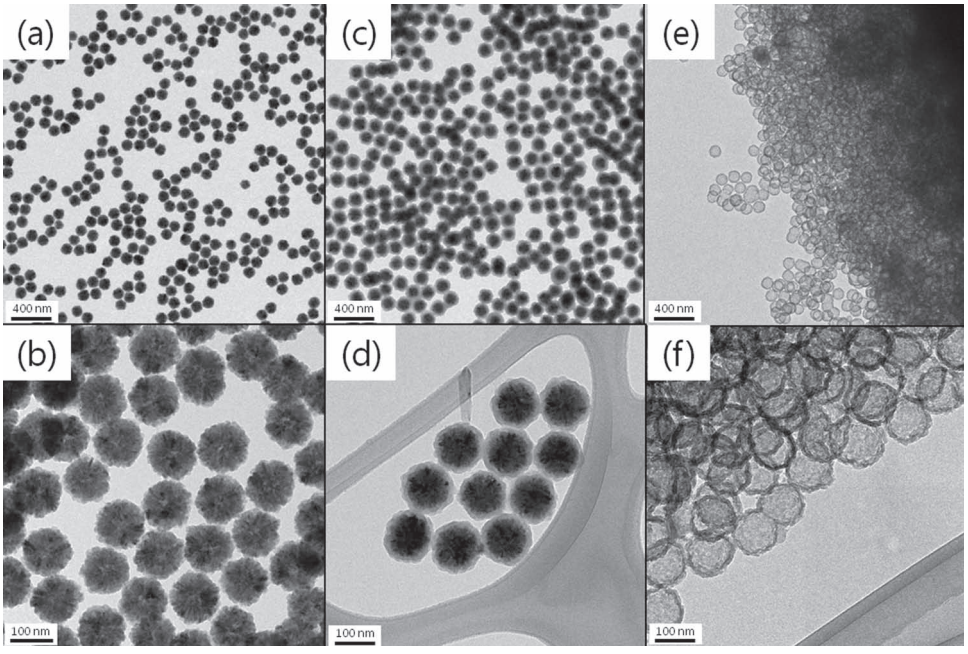

Figure 1. TEM images of a) ZnS particles, c) silica-coated ZnS particles, and e) hollow silica particles after removing the ZnS-core. b,d,f) are magnified views of (a), (c), and (e).

© 2012 WILEY-VCH Verlag GmbH & Co. KGaA, Weinheim

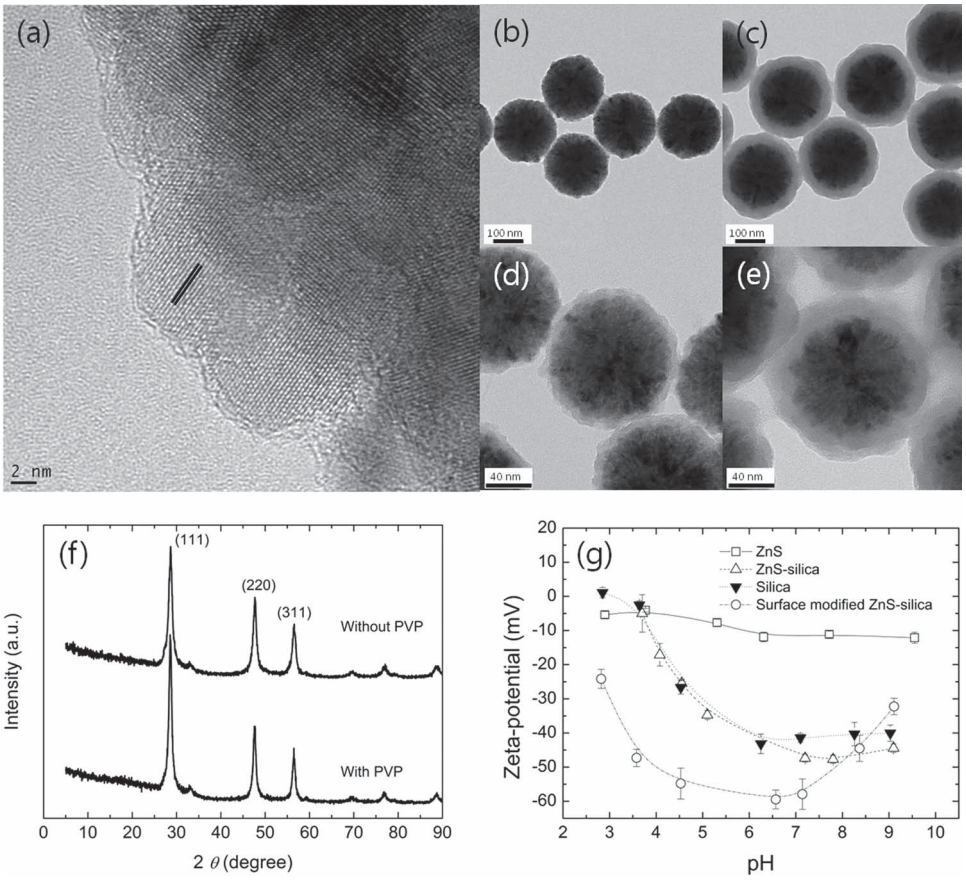

Figure 2. a) High resolution TEM image of a ZnS particle showing the nanocrystalline domains. b,c) TEM micrographs of ZnS particles and silica-coated ZnS particles whose particle sizes are larger than the particles presented in Figure 1. d,e) TEM micrographs of core–shell structures with different silica shell thicknesses formed by simply changing the total amount of feed TEOS in the synthetic recipes. f) Wide angle X-ray diffraction pattern of particles produced with and without PVP. g) Zeta-potential vs solution pH of pure ZnS particles (□), ZnS–silica particles (□), silica particles (▼), and surface-modified ZnS–silica particles (○).

confirmed by dynamic light scattering (DLS) (standard deviation was < 3%). The monodisperse nature of the ZnS particles is strong evidence that they form by a homogeneous nucleation process. As shown in **Figure 2**b, larger particles (≈200 nm) can also be synthesized by lowering the temperature to 60 °C. As measured by X-ray diffraction (Figure 2f), the crystal structure of the monodisperse nanoparticles is the same as that of ZnS polydisperse particles synthesized in the absence of PVP. The X-ray diffraction pattern reveals peaks at 28.5°, 47.5°, and 56.3°, corresponding to the (111), (220), and (311) planes, respectively, of the cubic zinc blende phase of ZnS,[26] indicating that the PVP does not change the crystal structure. As is observed in the high-resolution transmission electron microscopy (TEM) image (Figure 2a), the well-ordered lattice spacing is around 0.28 nm, corresponding to the (111) plane of the cubic ZnS phase.

The next step was to coat the surface of the ZnS nanoparticles with silica to endow a surface charge on the particle to increase the long-range electrostatic interactions. The surface zeta potential of the ZnS particle was found to be around –5 mV over a wide pH range (Figure 2g), which is not sufficient for forming a crystalline colloidal array. The pH independent weakly negative surface charge implies that the surface of the ZnS particle was effectively covered with PVP because intrinsic ZnS particles are observed to be negatively charged below pH of 6 with an iso-electric point of ZnS around pH 6.[27] The thin PVP layer on the ZnS functioned as a good anchoring material for the deposition of silica on the surface of the ZnS particle. The ZnS colloids could be uniformly coated with silica in an ethanol solution using ammonia as a catalyst through slow hydrolysis of tetraethyl orthosilicate (TEOS) according to the well-known Stöber process. After coating with silica, the zeta potential value was about –48 mV. Surface coating appears to be almost 100% as is shown in the TEM micrographs of the silica-coated particle in Figure 1c. Figure 1d indicates that it was possible to deposit ≈10 nm of a very even silica layer on the ZnS nanoparticle. The silica coating could be observed more noticeably after removing the ZnS core with 10 wt% of hydrazine (Figure 1e and f). Not surprisingly, the thickness of the coated layer could be effectively controlled by manipulating the feed ratios between ZnS and TEOS. The TEM micrograph in Figure 2d indicates a 5 nm silica layer on the ZnS particle, while Figure 2e shows a silica coating over 20 nm.

Although the ionization of the surface hydroxy groups of the SiO_2 provides a negative charge on the particle, they

© 2012 WILEY-VCH Verlag GmbH & Co. KGaA, Weinheim

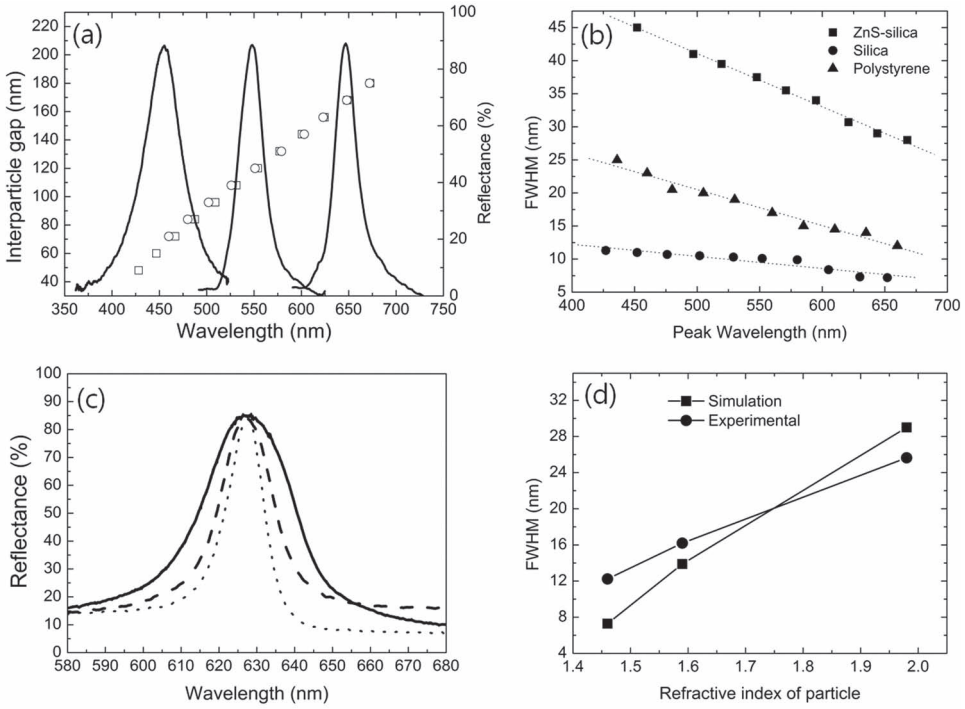

Figure 3. a) Left axis: relationship between inter-particle distance and reflectance peak position of crystalline colloidal arrays composed of ZnS–silica core–shell particles dispersed at different particle concentrations (□: calculated from Bragg equation, ○: calculated from FDTD simulation). Right axis: reflectance peaks exhibiting red, green, and blue colors. b) Simulated results showing relationships between bandwidth and peak wavelength of the crystalline colloidal arrays of silica, PS, and ZnS–silica in water obtained from the FDTD method. c) Experimental reflectance peaks exhibiting spectrum width at around 630 nm for silica (dotted line), PS (dashed line), and ZnS–silica (solid line).d) Comparison of simulated and experimented bandwidths vs. particle refractive index.

only partially dissociate in deionized water (pH 7) because the silanol groups are only weakly acidic. Under these conditions, the surface charge was not sufficient for the particle to induce repulsive interactions strong enough to self-assemble into long-range ordered crystalline colloidal arrays. Therefore, a silane coupling agent, 2-(4-chlorosulfonylphenyl)ethyltrimethoxysilane, was grafted onto the SiO_2 surface by hydrolysis of its methoxy group, and the chlorosulfonyl group ($–SO_2Cl$) was hydrolyzed in situ to the corresponding negatively charged sulfonic acid group.[28] The zeta-potential of the surface-modified ZnS–silica particle (Figure 2g) reached about –60 mV at a pH near 7, while the zeta-potential curve of the unmodified silica-coated ZnS particles was similar to that of silica particles. This data offers good evidence that the surface was changed after grafting.

The highly charged monodisperse ZnS–silica colloids were then self-assembled into crystalline colloidal arrays at high particle concentrations (greater than 4.8 vol%) and low ionic strength conditions. These charge-stabilized suspensions exhibited structural ordering at much lower volume fractions compared with sterically stabilized suspensions due to strong electrostatic repulsion between the particles caused by overlapping of the electrical double layer on the particles, resulting in relatively long-range interactions.[14–16] The high negative charge conferred on the surface of the particle and the resulting strong electrostatic repulsive force between the particles allowed us to prepare a photonic crystal with a photonic stop-band located in the full visible spectrum regime by manipulating the particle concentrations. **Figure 3**a shows the strong (~90% reflection) red, green, and blue structural colors obtained from ZnS–silica particles dispersed in water at particle concentrations of 21.9 (blue), 9.3 (green), and 5.4 (red) vol%, together with the interparticle spacings calculated using the Bragg equation and by the finite-difference time-domain (FDTD) simulation. The inter-particle gap of ≈160 nm at the reflectance peak position of around 630 nm indicates that the electrical double layer of the particle was at least 160 nm.

The photonic crystal diffraction wavelengths and the diffraction bandwidths depend on the periodicity of the refractive index modulation and the modulation depth.[29] In particular, the modulation of the refractive index contrast is important in controlling the stop-band width.[30] To investigate the effect of the refractive index contrast on the width of the stop-band, we prepared highly charged polystyrene (PS) (refractive index of 1.59) and silica (refractive index of 1.46) particles with diameters of 120 nm for the reference samples. The FDTD method calculated stop-band positions and the bandwidths of the crystalline colloidal arrays composed of ZnS–silica particles in water are compared in Figure 3b, assuming periodically positioned particles of 120 nm in size with different refractive indices[31] and different inter-particle spacings. The FDTD simulation results clearly suggest that the higher refractive index contrast produces a wider bandwidth and that the bandwidth increases with a shift in the stop-band position to a shorter wavelength. This

© 2012 WILEY-VCH Verlag GmbH & Co. KGaA, Weinheim

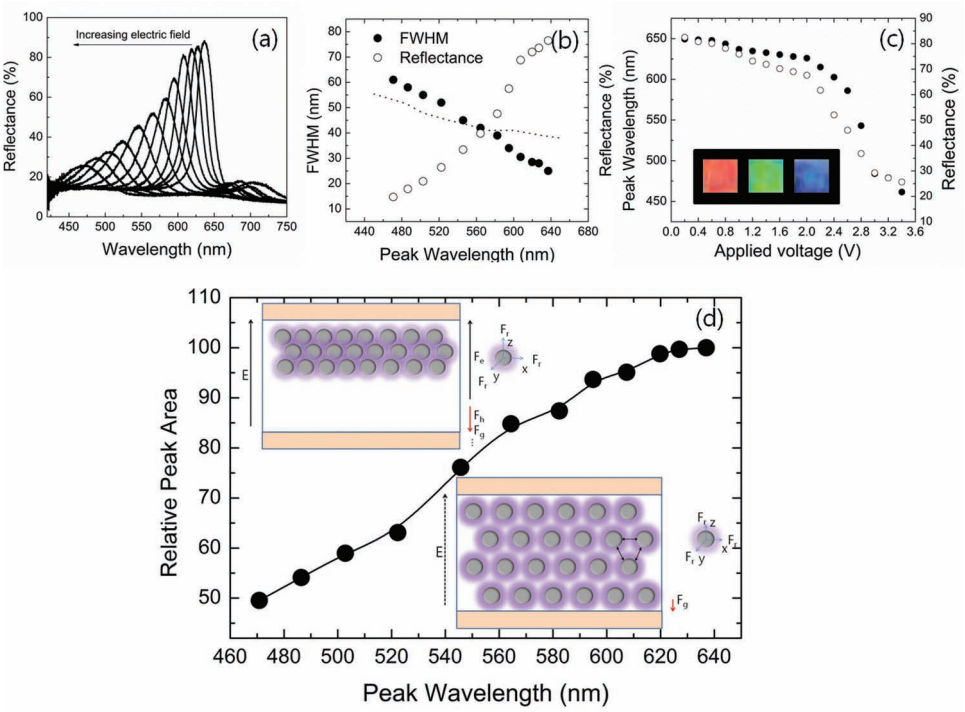

Figure 4. Photonic stop-band tuning behavior of ZnS–silica dispersed in water. a) A demonstration of the shift of reflectance spectrum with increasing voltages from 0 to 3.2 V. The ITO–ITO separation in the test cell is 100 μm. b) The peak reflectance and the peak FWHM as a function of the peak wavelength. The simulated value of FWHM is included as a reference (dotted line). c) Relationship between applied voltage vs. reflectance (○) and peak position (●). d) The calculated relative peak area at each peak position as a function of the peak wavelength (●). In the inset of (d), a possible mechanism for the stop-band position shift is schematically illustrated. Before the electrical potential is applied, the colloidal particle shows a periodic fcc structure due to repulsive forces in all directions. After an electrical potential is applied, the particles experience a strong electrophoretic force normal to the anode (+*z* direction) together with other forces such as hydrodynamic forces in the opposite direction (–*z* direction).

supports our strategy for increasing total reflection by modulating the refractive index contrast to meet the requirements of reflective displays.

Figure 3c provides experimental results for the effect of refractive index on peak width. The results clearly demonstrate that the reflectance peak at 630 nm widened with increasing particle refractive index. Comparison of the simulated results with the experimental results (Figure 3d) revealed fairly good agreement, although the simulated results had a tendency to be more sensitive to the changes in the refractive index. The reported theoretical[32,33] and simulated[34] bandwidth of crystalline colloidal arrays composed of negatively charged PS in water is very narrow (ca. 10 nm) and is close to our simulated and experimental results. This close agreement between the experimental and the calculated values and the similarity of the bandwidth with the reported values suggest good optical quality and uniformity of the long-range, self-assembled photonic crystal in our system. To our knowledge, there has been no report on the refractive index modulation of the particle using high refractive index materials. We also found that further modulation of the refractive index could be effectively obtained by controlling the volume ratios between the core and the shell (data not shown; compare Figure 1d, and Figure 2d,e).

Although the face centered cubic (fcc) structure of dielectric spheres in lower refractive index media only possess stop-gaps, the local density of the states can still be significantly manipulated and the photonic stop-band tuning can be realized even for quite modest index contrast. In our previous study,[35] high refractive index TiO_2 nanoparticles only exhibited a short-range interaction in ethylene glycol due to weak repulsive forces between particles. Hence, the manipulation of the stop-band position with electrical potential was impossible, and only the blue structural color could be switched when the particle spacing was modulated with electrical potential. A core–shell particle with a higher surface charge is expected to provide a system where stronger modulation of the optical properties with electrical potentials should be possible.

In the static state, the brilliant photonic structural color is mostly a result of strong electric double layer interactions between the nearest particles, which overcome the sedimental gravitational force of the particle to the direction of the negative electrode (cathode) that originates from the high density of the particle. These forces are balanced to exhibit a stable structural color. When an electrical potential is applied between the two indium tin oxide (ITO) electrodes in which the crystalline colloidal arrays consisting of highly charged ZnS–silica in aqueous solution are sandwiched, the force balance between the particles changes as is shown in the inset of **Figure 4**d. The electrophoretic force, which is attributable to the electrostatic Coulombic force to the positive electrode (anode), and the corresponding hydrodynamic force, which is due to the friction and the retardation force of the electrical double layer

© 2012 WILEY-VCH Verlag GmbH & Co. KGaA, Weinheim

of the particle[36] in the opposite direction, are added to the pre-existing forces. In this case, the electrophoretic force is the dominant force normal to the electrode (*z*-direction), and the particles move to the positive electrode. As a result, the average populations of the particles increase near the positive electrode while the general order of the particles is maintained due to their strong electrostatic repulsion. This leads to a shift in the photonic stop-band position to shorter wavelengths (Figure 4a). Full-color manipulation from red (peak position at 650 nm) to blue (peak position at 450 nm) has been achieved over the applied potential range of 0 to 3.2 V. It is noteworthy that increasing electric fields cause a stronger overlap between the electrical double layers of each particle, which is balanced by the applied electric field. This balance between the forces is what maintains the structure color at the desired stop-band position for a given applied potential.

Figure 4b shows the variation of the peak reflectance and the bandwidth as a function of the peak wavelength position at equilibrium for various applied electric fields. The bandwidth increased and the stop-band shifted to shorter wavelengths with increasing electric fields. This coincides well with the calculated value obtained by FDTD. The reflectance decreased with a shift in the stop-band to a shorter wavelength. Plotting the reflectance and the peak position against the applied potential (Figure 4c) revealed that both decrease in a similar fashion with increasing potential. The red, green, and blue colors resulting from stop-band tuning are also exhibited in the figure. The decrease in reflectance and the relative peak area (Figure 4d) is probably due to partial disorder resulting from inhomogeneous spacing between the colloidal layers along the *z*-direction (normal to the electrode), as noted in a previous report.[35] Detailed work on the colloidal modeling is underway to fully understand the mechanism of the tuning behavior. Due to the strong repulsive force between particles and the local high particle density, the colloidal system recovers to its original state when the potential is removed. This means that the manipulation of the position of the photonic stop-band is reversible, thereby offering a new strategy for the construction of bright full-color reflective displays.

In conclusion, highly charged silica-coated ZnS colloids were successfully produced and were self-assembled into long-range ordered crystalline colloidal arrays due to a strong electrostatic repulsion force between the particles. We have demonstrated that the reflectance spectrum width can be tuned through material engineering of the refractive index by adapting an approach of high-refractive index core/high-charge shell methodology. Using these crystalline colloidal arrays composed of engineered core–shell particles in water, active electrical tuning of the photonic stop-band in the whole range of the visible regime has been achieved. Our unprecedented results for full color tunability may pave the way toward developing full-color reflective displays with highly enhanced brightness under ambient light conditions.

Experimental Section

Synthesis of ZnS Nanoparticles: A representative synthetic procedure is as follows: Deionized water (200 mL) was charged into a flask and PVP (0.2 to 2 g) was added as a polymeric stabilizer, followed by stirring to completely dissolve. The temperature of the reactor was increased to 80 °C and TAA (0.1 mole) was added, followed by an addition of nitric acid (200 μL). Next, zinc nitrate hexahydrate (0.1 to 0.2 mole) was added and stirred for 3 h, and the resulting reaction completed the formation of the ZnS nanoparticles. The colloidal dispersions obtained were collected and purified by centrifuging and re-dispersing first in ethanol and then in water several times.

Preparation of ZnS–Silica Core–Shell Particles: Ammonia (3 mL) and deionized water (6 mL) were added to 80 mL of a 0.5 to 2 wt% ZnS colloidal solution and stirred for 1 h. TEOS (0.5 to 2 g) was added as a silica coating material and the reaction was carried out for 5 h at room temperature. The obtained core–shell particle was purified with repetitive centrifugation and re-dispersion at 8000 rpm and finally dispersed in ethanol at 1 vol%. The pH of the solution was adjusted to 4.8 by adding acetic acid. To the dispersion of 40 mL, ammonia (2 mL) and deionized water (1 mL) was added and stirred for 1 h followed by the addition of 2-(4-chlorosulfonylphenylethyltrimethoxysilane (20 μL). After reacting for 6 h, the colloids were purified again with a centrifugation and re-dispersion process.

Characterization and Stop-Band Tuning: TEM images were obtained with a 200 kV field emission TEM (Tecnai F20). The TEM specimens were prepared by dropping dilute dispersions of colloidal particles on a carbon-coated formva grid and dried. X-ray diffraction patterns were collected with Cu Kα radiation using an X'Pert PRO (Panalytical Inc.) from 5° to 90°. Zeta-potential measurements were performed over a range of pH values using a Brookhaven Zeta-plus instrument. The solution pH was adjusted with 10 mM of HCl and NaOH aqueous solution. DLS experiments for particle size distributions of the colloidal dispersion were carried out by a 90Plus/BiMAS (Brookhaven Co.). The wavelength of the incident laser beam (λ) was 532 nm and the detector angle (θ) was 90°. The core–shell particle was dispersed in de-ionized water at greater than 4.8 vol%, which is a critical concentration to exhibit reflective color. For example, 5.4 vol% exhibits a red structural color. After treating the colloidal dispersion with 10–50 vol% of ion-exchange resin (TMD-8 Mixed Bed Resin hydrogen and hydroxide form, Sigma–Aldrich), the colloidal dispersion exhibited a brilliant red color. The photonic crystal dispersion was then injected between two ITO electrodes separated by a 100 μm spacer. The optical properties of the photonic crystal layer were then measured using an Ocean Optics USB 4000 photo-diode array spectrophotometer during potential application. A Balanced Deuterium Tungsten Source (210–1700 nm) was used to illuminate samples through an optical fiber and the reflectance spectra were collected after calibrating the spectra against a STAN-SSH high reflectivity specular reflectance standard.

FDTD Simulation: Layers of crystalline colloidal arrays of fcc structure with different inter-particle spacing were used for modeling. The simulated models with three dimensions were periodic in the X and Y directions. A one-dimensional slab model of diffraction from the stack of (111) fcc crystal layers was developed by approximating each CCA layer with two slabs of different refractive indices. The models are illuminated by a normally incident plane wave. The particles with refractive indices of 1.46, 1.59, and 1.98, respectively, for silica, polystyrene, and ZnS–silica particle and a diameter of 120 nm were used to carry out simulations. Spectra of transverse electric and transverse magnetic waves were averaged with different inter-particle distances. Finally, the stop-band position and the bandwidth were calculated from the obtained optical spectra.

Acknowledgements

The authors thank Prof. Paul V. Braun (University of Illinois Urbana-Champaign) for his valuable technical advice and editing of this manuscript. The authors thank Dr. Hye Ran Choi for her excellent transmission electron microscopy work.

Received: August 4, 2012
Revised: August 20, 2012
Published online: October 9, 2012

© 2012 WILEY-VCH Verlag GmbH & Co. KGaA, Weinheim

[1] D. Graham-Rowe, *Nat. Photonics* **2007**, *1*, 248.
[2] B. Comiskey, J. D. Albert, H. Yoshizawa, J. Jacobson, *Nature* **1998**, *394*, 253.
[3] J. Heikenfeld, K. Zhou, E. Kreit, B. Raj, S. Yang, B. Sun, A. Milarcik, L. Clapp, R. Schwartz, *Nat. Photonics* **2009**, *3*, 292.
[4] D. Graham-Rowe, *Nat. Photonics* **2009**, *3*, 551.
[5] A. C. Arsenault, D. P. Puzzo, I. Manners, G. A. Ozin, *Nat. Photonics* **2007**, *1*, 468.
[6] J. Ge, Y. Hu, Y. Yin, *Angew. Chem. Int. Ed.* **2007**, *46*, 7428.
[7] Y. Kang, J. J. Walish, T. Gorrishnyy, E. L. Thomas, *Nat. Mater.* **2007**, *6*, 957.
[8] T. S. Shim, S.-H. Kim, J. Y. Sim, J.-M. Lim, S.-M. Yang, *Adv. Mater.* **2010**, *22*, 4494.
[9] M. Kolle, P. M. Salaard-Cunha, M. R. J. Scherer, F. Huanna, P. Vukusic, S. Mahain, J. J. Baumberg, U. Steiner, *Nat. Nanotechnol.* **2010**, *5*, 511.
[10] K. Chung, S. Yu, C.-J. Heo, J. W. Shim, S.-M. Yang, M. G. Han, H.-S. Lee, Y. Jin, S. Y. Lee, N. Park, J. H. Shin, *Adv. Mater* **2012**, *24*, 2375.
[11] M. Srinivasarao, *Chem. Rev.* **1999**, *99*, 1935.
[12] L. P. Biró, J. P. Vigneron, *Laser Photonics Rev.* **2011**, *5*, 27.
[13] C. I. Aguirre, E. Reguero, A. Stein, *Adv. Mater.* **2010**, *20*, 2565.
[14] P. A. Hiltner, I. M. Krieger, *J. Phys. Chem.* **1969**, *73*, 2386.
[15] J. H. Holtz, S. A. Asher, *Nature* **1997**, *389*, 829.
[16] M. G. Han, S. H. Foulger, *Adv. Mater.* **2004**, *16*, 231.
[17] L. D. Bonifacio, B. V. Lotsch, D. P. Puzzo, F. Scotognella, G. A. Ozin, *Adv. Mater.* **2009**, *21*, 1.
[18] K. P. Velikov, A. Moroz, A. van Blaaderen, *Appl. Phys. Lett.* **2002**, *80*, 49.
[19] J. Luo, D. Qu, A. Tikhonov, J. Bohn, S. A. Asher, *J. Colloid Interface Sci.* **2010**, *345*, 131.
[20] J. S. Steckel, J. P. Zimmer, S. Coe-Sullivan, N. E. Stott, V. Bulovic, M. G. Bawendi, *Angew. Chem. Int. Ed.* **2004**, *43*, 2154.
[21] R. N. Bhargava, D. Gallagher, X. Hong, A. Nurmikko, *Phys. Rev. Lett.* **1994**, *72*, 416.
[22] I. D. Hosen, C. M. Liddell, *Langmuir* **2007**, *23*, 2892.
[23] D. M. Wilhelmy, E. Matijevic, *J. Chem. Soc., Faraday Trans. 1* **1984**, *80*, 563.
[24] K. P. Velikov, A. van Blaaderen, *Langmuir* **2001**, *17*, 4779.
[25] Z. Q. Li, Y. Zhang, *Angew. Chem. Int. Ed.* **2006**, *45*, 7732.
[26] J. Nanda, S. Sapra, D. D. Sarma, *Chem. Mater.* **2000**, *12*, 1018.
[27] J. D. G. Duran, A. Ontiverso, E. Chibowski, F. Gonzalez-Caballero, *J. Colloid Interface Sci.* **1999**, *214*, 53.
[28] W. Wang, B. Gu, L. Liang, W. A. Hamilton, *J. Phys. Chem. B* **2003**, *107*, 12113.
[29] J. D. Joanopoulos, P. R. Villeneuve, S. Fan, *Nature* **1997**, *386*, 143.
[30] T. Kanai, T. Sawada, A. Toyotama, J. Yamanaka, K. Kitamura, *Langmuir* **2007**, *23*, 3503.
[31] Refractive index of ZnS–silica was calculated to be 1.98 by considering 100 nm ZnS core and 10 nm of silica coating following the equation; $\frac{R^3_{\text{core}}}{R^3_{\text{core-shell}}} \cdot n_{\text{core}} + \left(1 - \frac{R^3_{\text{core}}}{R^3_{\text{core-shell}}}\right) \cdot n_{\text{shell}}$, where R is a radius of the particle and n is a refractive index.
[32] R. J. Spry, D. J. Kosan, *Appl. Spectrosc.* **1986**, *40*, 782.
[33] J. F. Galisteo-Lopez, E. Palacios-Lidon, E. Catillo-Martinez, C. Lopez, *Phys. Rev. B* **2003**, *68*, 115109.
[34] L. Bechger, P. Lodahl, W. L. Vos, *J. Phys. Chem. B.* **2005**, *109*, 9980.
[35] H. Shim, J. Lim, C. G. Shin, S.-J. Jeon, M. G. Han, J.-K. Lee, *Appl. Phys. Lett.* **2012**, *100*, 063113.
[36] A. S. Khair, T. M. Squires, *Phys. Fluids* **2009**, *21*, 042001.

© 2012 WILEY-VCH Verlag GmbH & Co. KGaA, Weinheim